The TGFβ type I receptor TGFβRI functions as an inhibitor of BMP signaling in cartilage

Weiguang Wang[a], Hyelim Chun[b], Jongseung Baek[a], Joshua Elyahu Sadik[b], Anna Shirazyan[b], Peyman Razavi[b], Noah Lopez[b], and Karen M. Lyons[a,b,1]

[a]Department of Orthopaedic Surgery, University of California, Los Angeles, CA 90095; and [b]Department of Molecular Cell and Developmental Biology, University of California, Los Angeles, CA 90095

Edited by Richard M. Harland, University of California, Berkeley, CA, and approved June 25, 2019 (received for review February 18, 2019)

The type I TGFβ receptor TGFβRI (encoded by *Tgfbr1*) was ablated in cartilage. The resulting *Tgfbr1*^{Col2} mice exhibited lethal chondrodysplasia. Similar defects were not seen in mice lacking the type II TGFβ receptor or SMADs 2 and 3, the intracellular mediators of canonical TGFβ signaling. However, we detected elevated BMP activity in *Tgfbr1*^{Col2} mice. As previous studies showed that TGFβRI can physically interact with ACVRL1, a type I BMP receptor, we generated cartilage-specific *Acvrl1* (*Acvrl1*^{Col2}) and *Acvrl1/Tgfbr1* (*Acvrl1/Tgfbr1*^{Col2}) knockouts. Loss of ACVRL1 alone had no effect, but *Acvrl1/Tgfbr1*^{Col2} mice exhibited a striking reversal of the chondrodysplasia seen in *Tgfbr1*^{Col2} mice. Loss of TGFβRI led to a redistribution of the type II receptor ACTRIIB into ACVRL1/ACTRIIB complexes, which have high affinity for BMP9. Although BMP9 is not produced in cartilage, we detected BMP9 in the growth plate, most likely derived from the circulation. These findings demonstrate that the major function of TGFβRI in cartilage is not to transduce TGFβ signaling, but rather to antagonize BMP signaling mediated by ACVRL1.

BMP | TGFβ | cartilage | ALK1 | ALK5

Growth plate cartilage supports bone elongation and provides an essential platform for the generation of articular joints (1). Cartilage is generated by chondrocytes, which can be classified into different subtypes depending on their location and differentiation status (1). These subtypes form distinct zones in the growth plate. The pool of resting chondrocytes at the distal ends of developing long bones supplies cells for building growth plate cartilage. Resting chondrocytes differentiate into columnar chondrocytes, which have a high proliferative rate and stack together into columns. Columnar cells further differentiate into prehypertrophic chondrocytes, which cease proliferation and enlarge. These cells further differentiate into hypertrophic chondrocytes, which have a larger cell size and eventually undergo apoptosis or transdifferentiate into osteoblasts (2). Eventually, the growth plate is replaced by calcified bone.

TGFβ and bone morphogenetic protein (BMP) signaling components play important roles in cartilage and joint formation and maintenance (3–7). TGFβs 1 to 3 bind to complexes containing the type I receptor TGFβRI and the type II receptor TGFβRII. Ligand binding triggers phosphorylation of TGFβRI, enabling activation of the intracellular mediators SMADs 2 and 3 in the canonical TGFβ pathway. TGFβs also signal through activation of kinases such as MAP kinase, TAK1, JNK, and RhoA. BMPs are a diverse group of ligands that share homology to TGFβs 1 to 3, but bind to distinct receptor complexes consisting of type I (ACVRL1 [ALK1], ACVR1 [ALK2], BMPR1A [ALK6], and BMPR1B [ALK3]) and type II receptors (ACTRIIA, ACTRIIB, and BMPRII) (8). These complexes activate the intracellular SMADs 1/5/8 in the canonical pathway, as well as noncanonical pathways overlapping with those activated by TGFβ. In addition to shared noncanonical pathways, there is cross talk between TGFβ and BMP pathways at multiple levels (3, 9, 10).

Although the potent in vitro chondrogenic activity of TGFβs is well documented (11), the function of TGFβ pathways in cartilage in vivo is unclear. TGFβRII is the type II receptor for TGFβs 1 to 3. *Tgfbr2*^{Col2} mice exhibit axial skeletal defects but have no alterations in appendicular elements (12). Similarly, loss of *Smad3, Smad2*, or both in chondrocytes leads to no or only subtle growth plate phenotypes at birth (13, 14). These studies may not reflect all TGFβ pathway activity in committed chondrocytes. Targeting SMADs 2 and 3 leaves noncanonical pathways intact. Studies based on loss of TGFβRII may also underestimate TGFβ pathway activity; in cranial neural crest cells, TGFβs activate TGFβ signaling in the absence of TGFβRII (15). Furthermore, ligands other than TGFβs 1 to 3 (e.g., GDF8, GDF10, and GDF11) can activate signaling through TGFβRI in complexes containing ACTRIIA or ACTRIIB (16–18).

These findings raise the possibility that TGFβRI acts independently of TGFβRII in cartilage. A study of *Tgfbr1*^{Dermo1} mice showed that TGFβRI plays a critical role in formation of the perichondrium adjacent to the growth plate (19). Whether TGFβRI has a role in growth plate chondrocytes has not been investigated. TGFβRI is also of interest because it enables TGFβs to activate BMP signaling through a mechanism involving association of the BMP receptor ACVRL1 with TGFβRI/TGFβRII complexes (20, 21). TGFβ signaling through ACVRL1/TGFβRI/TGFβRII complexes augments BMP signaling in vascular cells (21). Whether such complexes exist in other tissues, and their impact on BMP signaling, is unclear.

Using mice lacking TGFβRI in cartilage (*Tgfbr1*$^{fx/fx}$*;Col2-Cre* [*Tgfbr1*^{Col2}]), we find that TGFβRI is required to maintain the pool of resting chondrocytes in the growth plate. Unexpectedly, the primary function of TGFβRI is not to activate TGFβ pathways. Rather, *Tgfbr1*^{Col2} mice exhibit elevated BMP activity

Significance

The TGFβ signaling pathway is activated when TGFβ ligands induce formation of TGFβRI and TGFβRII receptor complexes. However, loss of TGFβRI in mouse cartilage led to more severe defects than did loss of TGFβRII. Most of the defects were rescued by deletion of the BMP receptor ACVRL1, suggesting that a major role of TGFβRI in cartilage development is to suppress BMP signaling by ACVRL1. TGFβRI prevents the formation of ACVRL1/ACTRIIB complexes, which have high affinity for BMP9, the most abundant BMP in circulation. These results demonstrate a form of cross talk between BMP and TGFβ signaling pathways in cartilage that may also operate in other tissues where the relative output of these 2 pathways is required.

Author contributions: W.W. and K.M.L. designed research; W.W., H.C., J.B., J.E.S., A.S., P.R., and N.L. performed research; W.W., J.B., and K.M.L. analyzed data; and W.W. and K.M.L. wrote the paper.

The authors declare no conflict of interest.

This article is a PNAS Direct Submission.

[1]To whom correspondence may be addressed. Email: klyons@mednet.ucla.edu.

This article contains supporting information online at www.pnas.org/lookup/suppl/doi:10.1073/pnas.1902927116/-/DCSupplemental.

Published online July 16, 2019.

mediated by ACVRL1. Mechanistically, loss of TGFβRI triggers the formation of ACVRL1/ACTRIIB complexes in the growth plate. These have high affinity for the circulating BMP ligand BMP9, which we detected in growth plate cartilage. Thus, these studies indicate that the major function of the type I TGFβ receptor in growth plate cartilage is to prevent the promiscuous activation of ACVRL1-mediated BMP signaling by the circulating ligand BMP9.

Results

TGFβRI Is Expressed in Growth Plate Cartilage during Embryonic Development. We examined when and where TGFβRI is expressed to understand its potential roles in the growth plate. $Tgfbr1^{Col2}$ mice were used as negative controls for antibody specificity and confirmed that TGFβRI is efficiently deleted (*SI Appendix*, Fig. S1 *G* and *J*). At embryonic day 13.5 (E13.5), TGFβRI is expressed in intervertebral discs, and at lower levels in chondrocytes within vertebral bodies (*SI Appendix*, Fig. S1*A*). TGFβRI is expressed primarily in the perichondrium of appendicular elements at E13.5 but is present at low levels in chondrocytes (*SI Appendix*, Fig. S1 *B–E*). TGFβRI expression in appendicular growth plates is increased by E16.5 (*SI Appendix*, Fig. S1 *F* and *G*) and persists at least through E18.5 (*SI Appendix*, Fig. S1 *I* and *J*). Expression is strong at E16.5 and E18.5 in the columnar zone (CZ) but is absent from the hypertrophic zone (HZ) (*SI Appendix*, Fig. S1 *F* and *I*). At E16.5, resting chondrocytes in the developing posterior tibial condyle exhibit higher TGFβRI levels than do those in the anterior condyle (*SI Appendix*, Fig. S1*F* [yellow and white boxes] and *SI Appendix*, Fig. S1*H*). At E18.5, TGFβRI protein levels are high in resting zone (RZ) chondrocytes throughout the growth plate, and in the anterior and posterior condyles (*SI Appendix*, Fig. S1 *I* and *K*).

Severe Chondrodysplasia in *Tgfbr1* Mutant Neonates. Analysis of $Tgfbr1^{Dermo1}$ mice demonstrated a major role for TGFβRI in formation of the perichondrium (19). However, because *Dermo1-cre* is expressed in many mesodermal-derived tissues, whether TGFβRI had a direct function in chondrocytes could not be determined. We therefore generated $Tgfbr1^{f/f}$;*Col2-Cre* ($Tgfbr1^{Col2}$) mice to delete TGFβRI specifically in chondrocytes. The resulting $Tgfbr1^{Col2}$ mice exhibited perinatal lethality. The precise cause of death is unknown, but mutants exhibit major skeletal defects. At E13.5 and E14.5, there are no patterning defects in $Tgfbr1^{Col2}$ mice, but mutants have smaller vertebrae and occipital bones; no obvious defects in appendicular elements are seen at these stages (Fig. 1 *A* and *B*). At E16.5, defects in $Tgfbr1^{Col2}$ axial elements persist; mutants develop abnormal spinal curvature and kinks in the ribs at the chondro-osseous junction along with shortened sternebrae (Fig. 1*C*). There are no defects in appendicular patterning at E16.5, but long bones are shorter by this stage (Fig. 1 *E*, *F*, and *K*).

At E18.5, the severity of skeletal defects in the $Tgfbr1^{Col2}$ mice continues to progress. $Tgfbr1^{Col2}$ mice have shorter statures (E16.5: Mut/Ctrl, 87.2% ± 2%; E18.5: Mut/Ctrl, 73.9% ± 3%) and shorter tibiae than controls (Fig. 1 *C*, *D*, *F*, *H*, *K*, and *L*). E18.5 $Tgfbr1^{Col2}$ mice have bent scapulae, kinks at the distal ends of humeri, and dislocation of elbow joints (Fig. 1 *G* and *I*); these defects are not present at E16.5 (Fig. 1*E*). The condyles and entheses of tibiae are also smaller in mutants at E18.5 (Fig. 1 *H* and *J*). The proximal tibial cartilage is no different in length (Fig. 1*M*), but is wider in $Tgfbr1^{Col2}$ mice than in control littermates at E18.5 (Fig. 1*O*), and both the length and width of distal femoral cartilage are larger in $Tgfbr1^{Col2}$ mice (Fig. 1 *N* and *P*). As these defects are not seen in $Tgfbr2^{Col2}$ mutants (12) or $Smad2^{Col2}$/$Smad3^{-/-}$ mice (13), TGFβRI must transduce its effects in chondrocytes in combination with a different type II receptor, and through a pathway other than the canonical TGFβ pathway.

Chondrocyte Proliferation and Differentiation Defects in *Tgfbr1* Mutant Growth Plate Cartilage. We performed histological analyses to investigate mechanisms underlying the $Tgfbr1^{Col2}$ phenotype.

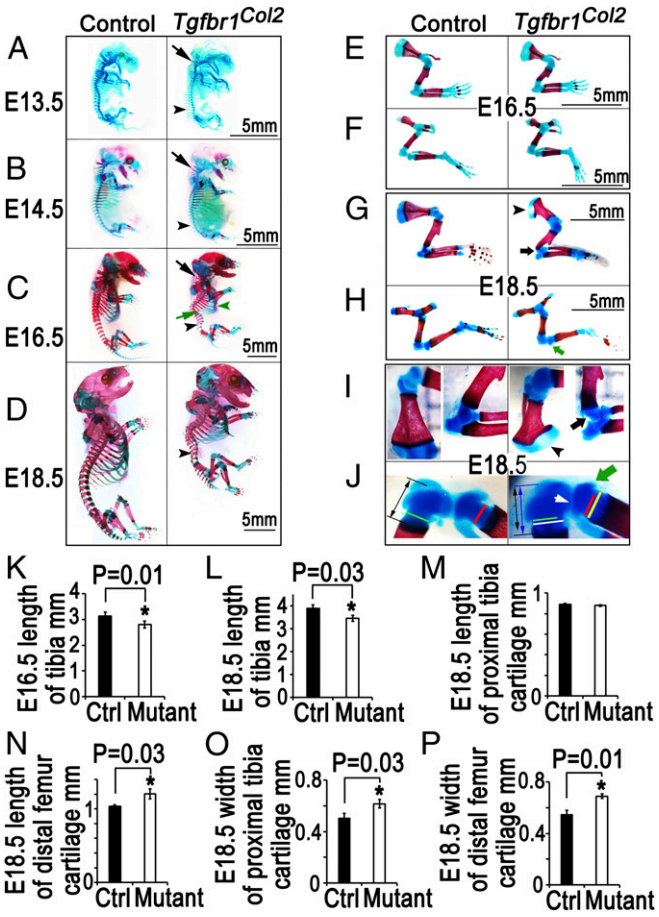

Fig. 1. Skeletal malformation in $Tgfbr1^{Col2}$ mice. (*A–D*) Cleared skeletal preparations of E12.5, E13.5, E16.5, and E18.5 control and *Tgfbr1* mutant embryos. Lateral views of littermates demonstrating that spine malformations can be detected in *Tgfbr1* mutants by E13.5 and become more severe at E18.5 (n = 5). Blue shows Alcian blue staining of cartilage. Red shows Alizarin red staining of bone. Control = $Tgfbr1^{fx/fx}$;$Tgfbr1^{Col2}$ = $Tgfbr1^{fx/fx}$;*Col2a1Cre*; black arrows in *A–C* denote the reduced sizes of cervical vertebral elements in mutants; black arrowheads in *A–D* denote the smaller, flatter lumbar vertebral bodies in $Tgfbr1^{Col2}$ mice. Green arrow in *C* denotes the locations of kinks in rib elements. Green arrowhead in *C* denotes the shortened sternebrae in *Tgfbr1* mutants. (*E–H*) Lateral views of E16.5 (*E* and *F*) and E18.5 (*G* and *H*) forelimbs (*E* and *G*) and hindlimbs (*F* and *H*), demonstrating the short humerus, femur, and tibia in *Tgfbr1* mutants compared with control littermates (n = 5). Black arrowhead points out the malformation of scapulae; black arrow denotes the dislocation of elbow joints; green arrow points out the small tibial condyles in E18.5 *Tgfbr1* mutant mice. (*I*) Magnified views of the defects in E18.5 scapulae and elbow joints in *Tgfbr1* mutant mice shown in *G*. Black arrowhead points out the malformation of scapulae and black arrow denotes the dislocation of elbow joints in *Tgfbr1* mutant mice. (*J*) Magnified views of the defects in E18.5 knee joints in *Tgfbr1* mutant mice shown in *H*. Black and blue double-headed arrows measure the length of control and *Tgfbr1* mutant femoral cartilage, respectively. Green and white bars measure the widths of the neck of femoral cartilage of control and *Tgfbr1* mutants, respectively. Red and yellow bars measure the widths of the neck of tibial cartilage of control and *Tgfbr1* mutants, respectively. The white arrow points out the flattened posterior tibial condyle in mutants; the green arrow shows the smaller anterior tibial condyle in mutants. (*K* and *L*) Quantification of the total lengths of tibiae in E16.5 and E18.5 control and *Tgfbr1* mutant embryos. n = 5 mice. Columns indicate average length of cartilage elements. Error bar shows SD. *P < 0.05; Student's 2-tailed t test. (*M* and *N*) Quantification of the length of tibial and femoral cartilages at knee joints in E18.5 control and *Tgfbr1* mutant embryos. n = 5 mice. Columns indicate average length of cartilage elements. Error bar shows SD. *P < 0.05; Student's 2-tailed t test. (*O* and *P*) Quantification of the widths of tibial and femoral cartilages at knee joints in E18.5 control and *Tgfbr1* mutant embryos. n = 5 mice, Columns indicate average length of cartilage elements. Error bar shows SD. *P < 0.05; Student's 2-tailed t test.

DEVELOPMENTAL BIOLOGY

The RZ is a sparsely dividing reservoir of cells that gives rise to the actively proliferating cells of the CZ (1). *Tgfbr1*^{Col2} mice have shorter RZs and longer CZs (Fig. 2 *A* and *B*) at E16.5 and E18.5 (Fig. 2 *C*, *D*, *G*, and *H*), although the lengths of HZ and the total growth plate do not differ in *Tgfbr1*^{Col2} and control littermate mice (Fig. 2 *E*, *F*, *I*, and *J*). Immunostaining for proliferating cell nuclear antigen (PCNA) revealed that levels of proliferation are higher in the CZ and RZ in *Tgfbr1*^{Col2} mice (Fig. 2 *K* and *L*). These results suggest that loss of *Tgfbr1* leads to premature conversion of slowly dividing RZ cells into rapidly proliferating CZ cells and depletion of the RZ (Fig. 2 *K* and *L*). Terminal deoxynucleotidyltransferase deoxyuridine triphosphate nick-end labeling (TUNEL) assay was performed to test whether increased apoptosis also contributes to the shorter RZ and smaller tibial condyles in *Tgfbr1*^{Col2} mice. No TUNEL-positive cells are seen in *Tgfbr1*^{Col2} RZ and in condyles; strong TUNEL staining is present only in the terminal HZ and adjacent perichondrium (Fig. 2*M*). No differences are observed in *Tgfbr1*^{Col2} and control littermate mice in these areas (Fig. 2*N*).

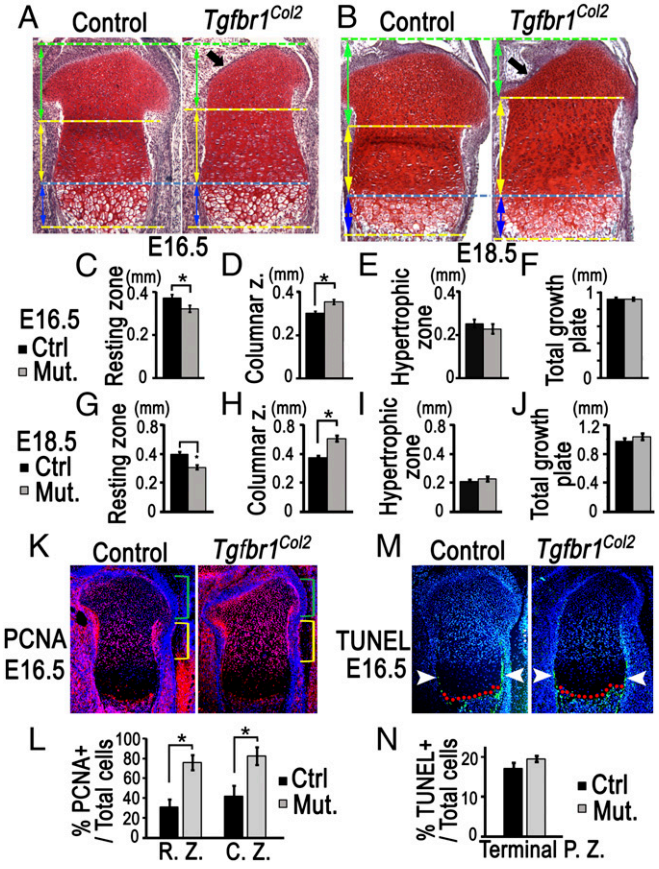

Fig. 2. Increased proliferation in *Tgfbr1* mutant growth plates. (*A* and *B*) Sections of E16.5 and E18.5 proximal tibias were stained with safranin O, showing reduced RZ and expanded CZ. Heights of different growth plate zones are indicated by double arrows, and the zone boundaries are marked by lines. Blue dashed line is the demarcation between the CZ and pre-HZ. All images are aligned to this boundary. Top yellow lines demarcate the approximate boundary between the RZ and CZ. Bottom yellow lines demarcate the boundary between the HZ and zone of ossification (chondro-osseous junction). Yellow double-headed arrows indicate the extent of the CZ. Green double-headed arrows demarcate the extent of the RZ. Blue double-headed arrows demarcate the extent of the HZ. Three litters containing mice of all of the genotypes shown in the figures were examined. At least 5 mice per genotype were examined. The images shown are from littermates. Black arrow highlights absence of the PCL enthesis. (*C*–*J*) Quantification of the lengths of different zones and whole growth plates. Data are expressed as means of length + SD (n = 5 mice). *$P < 0.05$; Student's 2-tailed t test compared with control *Tgfbr1*$^{fx/fx}$. (*K*) Immunostaining for PCNA (red) in E16.5 proximal tibia. RZ (green brackets) and CZ (yellow brackets). All mice are littermates. (*L*) Quantitation of the percentage of PCNA-positive cells in distinct zones. The percentage of PCNA-positive cells in the RZ and CZ was quantified. Data are expressed as means of percent PCNA-positive + SD (n = 4 mice). *$P < 0.05$ compared with control *Tgfbr1*$^{fx/fx}$ mice. (*M*) TUNEL (green) staining in E16.5 proximal tibia. All mice are littermates. White arrowheads point to perichondrium. Red dotted lines indicate chondro-osseous junction. (*N*) Quantitation of the percentage of TUNEL-positive cells at chondro-osseous junctions. Data are expressed as means of percent TUNEL-positive + SD (n = 4 mice). There are no significant differences between *Tgfbr1*^{Col2} and control *Tgfbr1*$^{fx/fx}$ mice.

Increased BMP Signaling in Growth Plate Cartilage. TGFβRI can trigger multiple downstream pathways, including SMAD2/3-mediated canonical signaling, TAK1-mediated noncanonical signaling, and SMAD1/5/8-mediated BMP signaling (8, 9, 20, 21). Immunostaining showed that there is a significant decrease in the percentage of p-SMAD2/3–positive cells in *Tgfbr1*^{Col2} growth plates (Fig. 3 *A* and *B*). However, *Smad2* and *Smad3* mutants do not have any of the defects seen in *Tgfbr1*^{Col2} growth plates (13), suggesting that the decrease in p-SMAD2/3 is not a major contributor to the *Tgfbr1*^{Col2} phenotype. Similarly, TAK1 is required in growth plate cartilage to activate proliferation (22). In palatal mesenchyme, TGFβ2 activates TAK1 independently of TGFβRII through TGFβRI (15). However, immunostaining revealed no difference in pTAK1 expression in *Tgfbr1*^{Col2} mice (Fig. 3 *C* and *D*).

Multiple studies indicate that BMP signaling triggers proliferation of RZ and CZ chondrocytes (23–25). Because the growth plate defects in *Tgfbr1*^{Col2} mice are consistent with elevated BMP signaling and cannot be explained by decreased activation of TGFβ pathways, we considered the possibility that BMP signaling is altered. Immunostaining for pSMAD1/5/8 revealed an increased percentage of pSMAD1/5/8-positive cells in the RZ and CZ of *Tgfbr1*^{Col2} mice (Fig. 3 *E* and *F*). The increased pSMAD1/5/8 levels do not arise through increased mRNA expression of key BMP, TGFβ, or GDF ligands, BMP type I or type II receptors, the BMP inhibitor NOGGIN, or the BMP signaling mediators SMAD1, SMAD5, and SMAD8 (*SI Appendix*, Fig. S2).

Loss of *Acvrl1* Rescues Growth Plate Defects in *Tgfbr1*^{Col2} Mutant Mice. The above findings indicated that TGFβRI acts to inhibit BMP signaling in growth plate cartilage. In considering potential mechanisms, we focused on the type I BMP receptor ACVRL1 (ALK1). ACVRL1 has been studied almost exclusively in the context of the vasculature, because heterozygous loss-of-function mutations in *Acvrl1* lead to hereditary hemorrhagic telangiectasia in humans (26). However, *Acvrl1* is expressed in articular cartilage (27, 28). ACVRL1 can interact physically with TGFβRI and TGFβRII to enable TGFβ ligands to activate BMP signaling (21). According to this model, loss of TGFβRI would lead to decreased BMP signaling, opposite to the elevated BMP signaling observed in *Tgfbr1*^{Col2} growth plates. We therefore speculated that an alternative function for TGFβRI could be to inhibit BMP signaling through ACVRL1. This might occur if TGFβRI prevents formation of highly active (ACVRL1/ACTRIIA or ACVR1/ACTRIIB) complexes by sequestering ACVRL1 into less active complexes containing TGFβRI.

ACVRL1 is expressed in all zones of the growth plate (Fig. 4*A*). To test the role of ACVRL1 in cartilage and whether there is a genetic interaction between *Tgfbr1* and *Acvrl1*, we generated *Acvrl1*$^{f/f}$*;Col2-Cre* (*Acvrl1*^{Col2}) and *Acvrl1*/*Tgfbr1* double-mutant *Acvrl1*$^{f/f}$*;Acvrl1*$^{f/f}$*;Col2-Cre* (*Acvrl1*/*Tgfbr1*^{Col2}) mice. Cartilage-specific deletion of *ACVRL1* was confirmed by immunohistochemistry (IHC) (Fig. 4*B*). *Acvrl1*^{Col2} mice are apparently normal at E18.5 (Fig. 4 *C* and *D*). Histological analysis showed that *Acvrl1*^{Col2} mice have normal growth plates (Fig. 4 *G* and *H*), and no changes in pSMAD1/5/8 levels were detected (Fig. 4 *K* and *L*). Strikingly, however, simultaneous loss of *Acvrl1* and *Tgfbr1* rescues most of the skeletal defects seen in *Tgfbr1*^{Col2} mice (Fig. 4 *E* and *F*). The length of the CZ (Fig. 4 *G*, *I*, and *J*) and

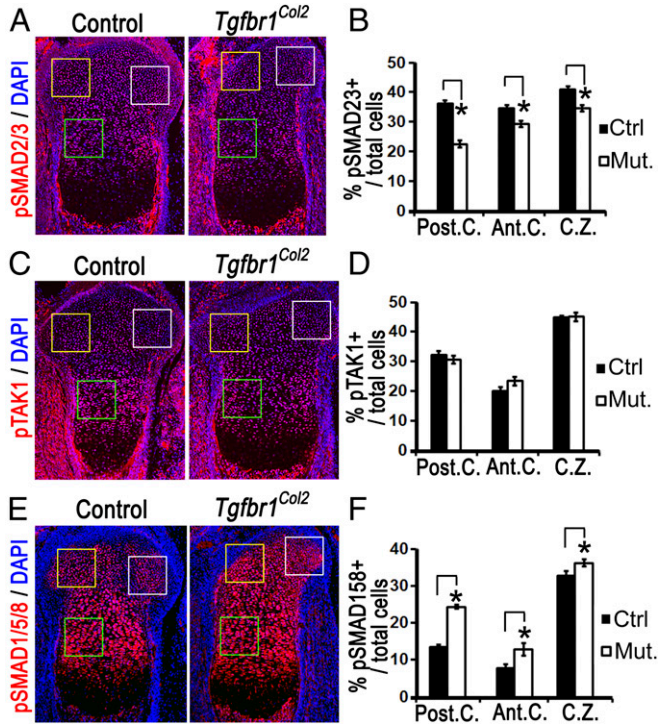

Fig. 3. Increased BMP signaling activity in *Tgfbr1* mutant growth plates. All images are E16.5 proximal tibias. Quantification data are expressed as means + SD ($n = 3$ mice). *$P < 0.05$; Student's 2-tailed t test. (*A* and *B*) Immunostaining for phosphorylated SMAD2 and SMAD3 showing decreased protein levels in *Tgfbr1* mutant growth plates. (*B*) Quantification of pSMAD2/3 protein level in posterior condyles (yellow boxes), anterior condyles (white boxes), and CZs (red boxes) of growth plate. (*C* and *D*) Immunostaining for phosphorylated TAK1 (pTAK1) showing no change of expression levels in *Tgfbr1* mutant growth plates. (*D*) Quantitation of pTAK1 protein level in the posterior condyles (yellow boxes), anterior condyles (white boxes), and CZs (red boxes) of growth plate. (*E* and *F*) Immunostaining for phospho-SMAD1/5/8 protein showing increase levels of activated BMP signaling in *Tgfbr1*^{Col2} growth plates. (*F*) Quantitation of pSMAD1/5/8 protein level in the posterior condyles (yellow boxes), anterior condyles (white boxes), and CZs (red boxes) of growth plate.

pSMAD1/5/8 levels (Fig. 4 *K*, *M*, and *N*) are restored to normal in *Acvrl1*/*Tgfbr1*^{Col2} mice. However, the rescue of *Tgfbr1*^{Col2} defects is not complete. Vertebral bodies remain smaller than control littermates in *Acvrl1*/*Tgfbr1*^{Col2} mice (Fig. 4 *C*, *E*, and *F*; arrowheads), and the enthesis defects are not fully rescued (Fig. 4 *G*, *I*, and *J*; arrows). These defects could reflect a role for TGFβRI in transducing TGFβ pathways, and/or interactions between TGFβRI and type I BMP receptors other than ACVRL1 in these regions. Nonetheless, these results demonstrate that *Acvrl1* is not necessary for growth plate formation, but interacts genetically with *Tgfbr1*, and that TGFβRI antagonizes ACVRL1 function in the growth plate.

TGFβRI Associates with ACVRL1 and ACTRIIB to Inhibit ACVRL1/ACTRIIB Complex Formation. The genetic studies demonstrated that a key function for TGFβRI is to constrain ACVRL1 signaling in the growth plate. ACVRL1 normally complexes with ACTRIIA/B to transduce BMP9/10-activated SMAD1/5/8 BMP signaling (29). TGFβRI complexes with ACTRIIA/B transduce GDF8/11-activated SMAD2/3 TGFβ signals (16, 18). Therefore, competition between ACVRL1 and TGFβRI for ACTRIIA and/or ACTRIIB provides a potential explanation for the elevated BMP signaling in *Tgfbr1*^{Col2} mice and its rescue in *Acvrl1*/*Tgfbr1* double mutants. We performed coimmunoprecipitation (co-IP) in ATDC5 chondrocytes under serum-free conditions to identify endogenous TGFβRI interactions with type I and type II BMP receptors. Among the type I BMP receptors, TGFβRI associates primarily with ACVRL1 (Fig. 5 *A* and *B*). A low level of association of TGFβRI with ACVR1, the type I receptor most closely related structurally to ACVRL1 (8), was detected; almost no association with BMPR1A or BMPR1B was found. Proximity ligation assay (PLA) confirmed that the observed interaction between TGFβRI and ACVRL1 occurs in vivo (*SI Appendix*, Fig. S5). Thus, the genetic interaction between ACVRL1 and TGFβRI is correlated with a physical interaction between these receptors in chondrocytes. We next considered interactions with type II receptors. We focused on TGFβRII because TGFβRI/TGFβRII complexes transduce canonical signaling by TGFβs 1 to 3, and on ACTRIIA and ACTRIIB because these type II receptors can complex with either ACVRL1 or TGFβRI (3, 16, 18, 29). Among the tested type II receptors, TGFβRI associates exclusively with ACTRIIB under serum-free conditions (Fig. 5 *C* and *D*). The lack of association between TGFβRI and TGFβRII is consistent with the lack of a growth plate phenotype in *Tgfbr2*^{Col2} mice (12).

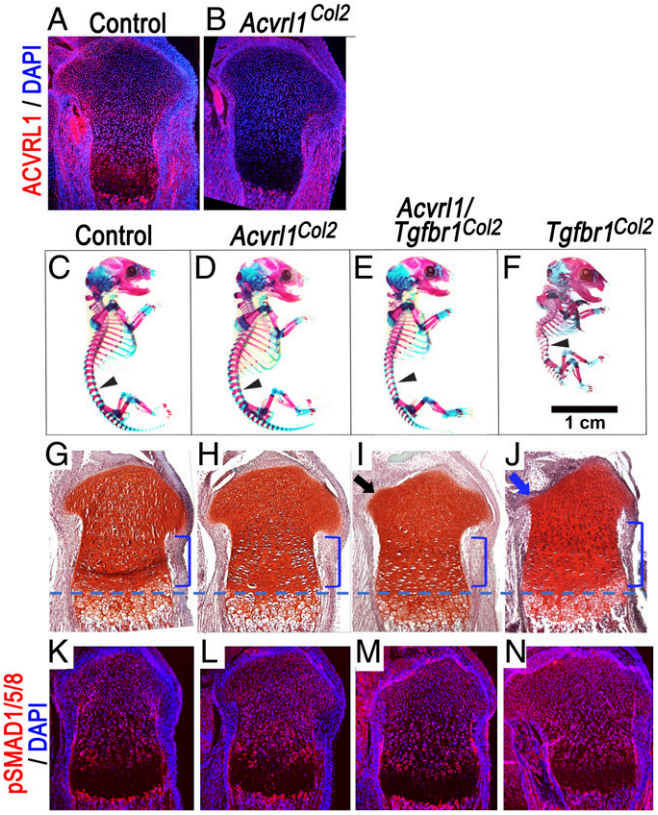

Fig. 4. Rescue of the *Tgfbr1* mutant phenotype in *Acvrl1*/*Tgfbr1*^{Col2} double mutants. All images are E18.5. (*A* and *B*) Immunofluorescent staining showing ACVRL1 protein presence in proximal tibial growth plates of control mice (*A*) and lack of staining in *Acvrl1* mutant mice (*B*) verifies antibody specificity and cartilage-specific knockout. Red, α-ACVRL1 staining; blue, DAPI. (*C*–*F*) Skeletal preps showing no alterations in *Acvrl1* ^{Col2} mice, and rescue of the chondrodysplasia in *Acvrl1*/*Tgfbr1*^{Col2} mice compared with *Tgfbr1*^{Col2} mice. Arrowheads point to the vertebral body (VB); note that there are no defects in *Acvrl1*^{Col2} VB, but both *Acvrl1*/*Tgfbr1*^{Col2} and *Tgfbr1*^{Col2} mice have smaller VB compared with control mice. $n = 5$/genotype. (*G*–*J*) Sections through proximal tibia growth plates showing restoration of the highs of the CZ and the sizes of posterior condyle in *Acvrl1*/*Tgfbr1*^{Col2} mice. Blue brackets indicate the high of CZ. Black arrow points to the rescued tibia condyle in *Acvrl1*/*Tgfbr1*^{Col2} mice. Blue arrow points to the defective of posterior tibial condyle in *Acvrl1*/*Tgfbr1*^{Col2} mice. $n = 3$/genotype. (*K*–*N*) pSMAD1/5/8 levels appear to be restored to normal in *Acvrl1*/*Tgfbr1*^{Col2} mice. $n = 3$/genotype.

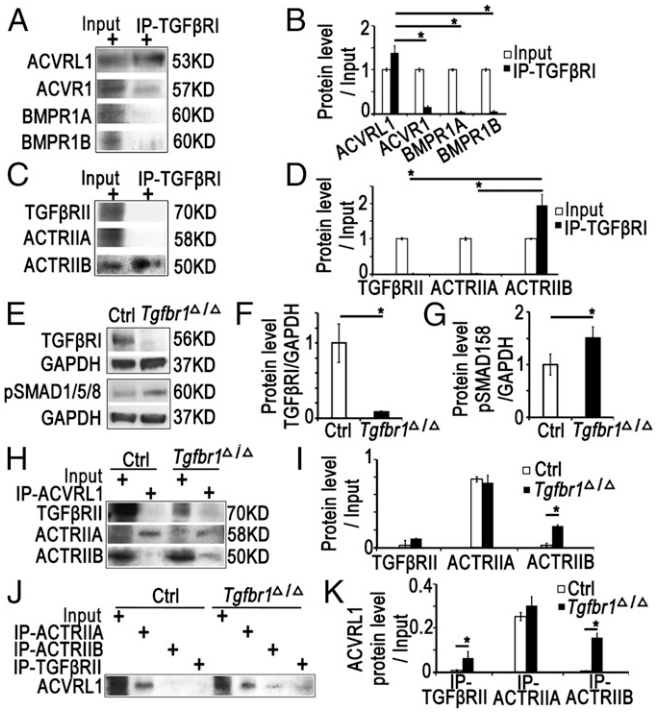

Fig. 5. TGFβRI associates with ACVRL1 and ACTRIIB to block ACVRL1/ACTRIIB complex formation. (*A*) TGFβRI associates most with ACVRL1. Lysates prepared from ATDC5 cells were subjected to IP with an anti-TGFβRI antibody cross-linked to magnetic beads. Immunoprecipitated proteins were then probed with anti-ACVRL1, anti-ACVR1, anti-BMPR1A, and anti-BMPR1B antibodies. (*B*) Quantification of protein levels shown in *A*. Three biological replicates were analyzed. The average input protein level is normalized to 1. Immunoprecipitated protein level (IP-TGFβRI) was normalized using input and plotted relative to input + SD ($n = 3$). Significance was established using 2-way ANOVA and *t* test. $^*P < 0.013$. (*C*) Of the tested type II BMP receptors, TGFβRI associates almost exclusively with ACTRIIB. Immunoprecipitated proteins were probed with anti-TGFβRII, anti-ACTRIIA, and anti-ACTRIIB antibodies. Note that ACTRIIB, but not TGFβRII or ACTRIIA, could be coimmunoprecipitated with TGFβRI. (*D*) Quantification of protein levels shown in *C*. Three biological replicates were analyzed as described in *B*. $^*P < 0.017$. (*E*) Western blot images confirm that TGFβRI protein is deleted by Crispr-cas9 in *Tgfbr1* mutant ($Tgfbr1^{\Delta/\Delta}$) ATDC5 cells, and that these cells exhibit elevated basal pSMAD1/5/8 levels. (*F* and *G*) The Western blot images of TGFβRI (*F*) and pSMAD1/5/8 levels (*G*) were quantified using ImageJ. Values of protein level were normalized using GAPDH and are plotted relative to control + SD ($n = 3$ biological replicates). Significance was established using Student's 2-tailed *t* test. $^*P < 0.05$. (*H*) Lysates from control or $Tgfbr1^{\Delta/\Delta}$ cells were subjected to IP with an anti-ACVRL1 antibody. Immunoprecipitated proteins were then probed with anti-TGFβRII, anti-ACTRIIA, and anti-ACTRIIB antibodies. In control cells, ACVRL1 associates with ACTRIIA. In $Tgfbr1^{\Delta/\Delta}$cells, ACVRL1 associates with both ACTRIIA and ACTRIIB. (*I*) Quantification of protein levels shown in *E*. Three biological replicates were analyzed. Immunoprecipitated protein level was normalized using input and plotted relative to input + SD ($n = 3$). Significance was established using Student's 2-tailed *t* test. $^*P < 0.01$. Note that there is a significant increase of ACTRIIB/ACVRL1 association in $Tgfbr1^{\Delta/\Delta}$ cells compared with control cells. (*J*) Lysates from control or $Tgfbr1^{\Delta/\Delta}$ cells were subjected to IP with an anti-TGFβRII, anti-ACTRIIA, or anti-ACTRIIB antibody. Immunoprecipitated proteins were then probed with an anti-ACVRL1 antibody. In control cells, ACVRL1 associates with ACTRIIA. In $Tgfbr1^{\Delta/\Delta}$ cells, ACVRL1 associates with both ACTRIIA and ACTRIIB. (*K*) Quantification of protein levels shown in *G*. Three biological replicates were analyzed as described in *I*. $^*P < 0.05$. Note that there is a significant increase in ACTRIIB/ACVRL1 association in $Tgfbr1^{\Delta/\Delta}$ cells compared with control cells.

The association of TGFβRI with ACTRIIB in chondrocytes is consistent with potential competition between ACVRL1 and TGFβRI for this type II receptor. We generated *Tgfbr1* mutant ATDC5 cells ($Tgfbr1^{\Delta/\Delta}$) using Crispr-Cas9 systems to test this possibility. The removal of TGFβRI was confirmed by Western blot (Fig. 5 *E* and *F*). Elevated pSMAD1/5/8 levels were seen in $Tgfbr1^{\Delta/\Delta}$ cells even under serum-free conditions (Fig. 5 *E* and *G*), confirming that loss of TGFβRI leads to elevated BMP signaling in chondrocytes. Co-IP assays were performed to determine how loss of TGFβRI impacts association of ACVRL1 with type II receptors. In control cells, ACVRL1 associates primarily with ACTRIIA (Fig. 5 *H* and *I*). In $Tgfbr1^{\Delta/\Delta}$ cells, ACVRL1 associates with both ACTRIIA and ACTRIIB (Fig. 5*H*). Thus, loss of TGFβRI significantly increases the interaction of ACVRL1 with ACTRIIB (Fig. 5*I*). The increased formation of ACVRL1/ACTRIIB complexes is not caused by increased ACTRIIB protein levels because there is a similar level of input of ACTRIIB between control and $Tgfbr1^{\Delta/\Delta}$ cells (Fig. 5*H*). There is no change in ACVRL1/TGFβRII or ACVRL1/ACTRIIA complexes in $Tgfbr1^{\Delta/\Delta}$ cells compared with the control (Fig. 5*I*). Furthermore, there is a significant increase in ACVRL1/ACTRIIB interaction in $Tgfbr1^{\Delta/\Delta}$ cells compared with control cells after normalization to ACVRL1 input levels (Fig. 5 *J* and *K*). No changes in levels of ACVRL1/TGFβRII or ACVRL1/ACTRIIA complex formation were seen in $Tgfbr1^{\Delta/\Delta}$ cells (Fig. 5 *J* and *K*), suggesting that the increased formation of ACVRL1/ACTRIIB complexes is responsible for the elevated pSMAD1/5/8 levels in $Tgfbr1^{\Delta/\Delta}$ cells.

Loss of TGFβRI Increases Basal BMP Activity and BMP9 Responsiveness in Chondrocytes. The above findings demonstrated increased formation of ACVRL1/ACTRIIB complexes in $Tgfbr1^{\Delta/\Delta}$ cells. To test whether the ACVRL1/ACTRIIB complex has a specific function in mediating elevated BMP signaling in $Tgfbr1^{\Delta/\Delta}$ cells, cells were treated with BMP9, which acts exclusively through ACVRL1 or ACVR1 complexed to ACTRIIA or ACTRIIB, but shows significantly higher affinity for ACTRIIB than for ACTRIIA (29). TGFβ1 and BMP2 were used as controls because TGFβ1 can trigger BMP signaling through ACVRL1/TGFβRI/TGFβRII complexes (27). BMP2 activates BMPR1A and BMPR1B, and to a lesser extent ACVR1, but not ACVRL1 (8, 30–32). 12×SBE-Luc reporter assays showed that $Tgfbr1^{\Delta/\Delta}$ cells have higher basal BMP activity (2×) than control cells (1×), and increased responsiveness to BMP9 (5.8× vs. 3.3×) (significance confirmed by ANOVA and *t* test) (Fig. 6*A*). In contrast, responsiveness to BMP2 was slightly lower in $Tgfbr1^{\Delta/\Delta}$ (2.6×) compared with control cells (3.2×) (no significance by ANOVA and *t* test) (Fig. 7*A*). Consistent with the previously demonstrated requirement for TGFβRI in TGFβ-mediated BMP pathway activation (21), TGFβ1 stimulates BMP signaling in control, but not in $Tgfbr1^{\Delta/\Delta}$ cells. Taken together, these results indicate that loss of TGFβRI increases sensitivity to BMP9. Since the affinity of BMP9 for ACVRL1/ACTRIIB complexes is several orders of magnitude higher than for ACVRL1/ACTRIIA complexes (29), our results suggest that the increased formation of ACVRL1/ACTRIIB receptor complexes (Fig. 5) may be responsible for the increased responsiveness to BMP9 in $Tgfbr1^{\Delta/\Delta}$ cells.

As discussed, basal BMP activity is elevated in $Tgfbr1^{\Delta/\Delta}$ ATDC5 cells even under serum-free conditions. To test whether the elevated basal activity is due to production of an endogenous ligand, the BMP inhibitor NOGGIN (blocks BMPs 2, 4, 5, and 7, and GDFs 5 to 7) (33) was added to the cells followed by reporter assay. The elevated basal BMP activity in $Tgfbr1^{\Delta/\Delta}$ cells is not affected by NOGGIN; NOGGIN activity was confirmed by its ability to block the effects of recombinant BMP2 activity (Fig. 6*B*). NOGGIN does not inhibit BMPs 9 or 10, the ligands for ACVRL1 (34). To test whether the elevated basal BMP activity in $Tgfbr1^{\Delta/\Delta}$ cells is due to production of BMP9 or BMP10 and signaling through ACVRL1/ACTRIIB complexes, anti-BMP9 antibody, ACVRL1-Fc, or ACTRIIB-Fc was added to the cells. Anti-BMP9 antibody blocks BMP9 function (35, 36). ACVRL1-Fc and ACTRIIB-Fc bind to BMP9 and BMP10 (29, 37). While anti-BMP9 antibody, ACVRL1-Fc and ACTRIIB-Fc inhibit the effects of exogenous BMP9, they do not affect the elevated basal activity (Fig. 6 *C*–*E*). These results demonstrate that the increased BMP output is not due to increased

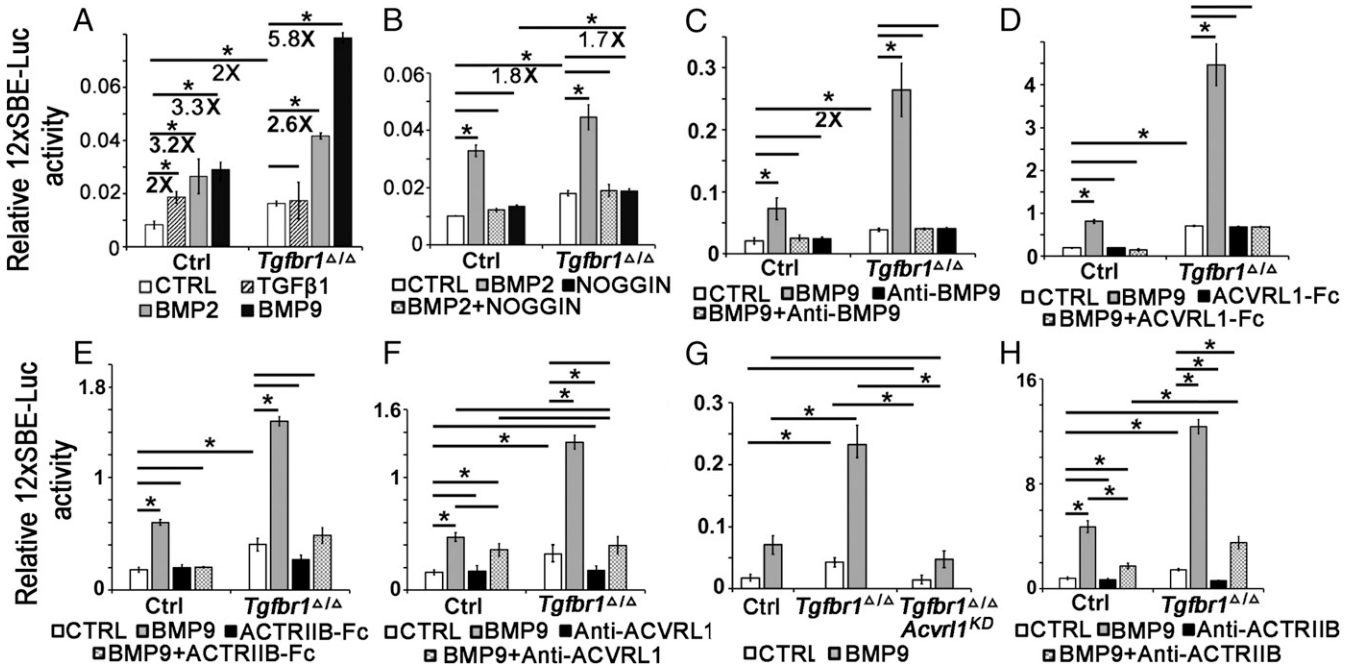

Fig. 6. Loss of TGFβRI leads to elevated basal BMP activity and BMP9 responsiveness in chondrocytes. Cells were transfected with 12×SBE-Luc reporter (77) and *Renilla* luciferase control reporter. Relative 12×SBE-Luc activity shows the normalized level of 12×SBE-Luc/*Renilla* Luc. Assays were repeated 2 times. n = 3/technical repeats in each assay. Error bars show SE. Significance was established using 2-way ANOVA and t test. $*P < 0.05/n$ (n = number of groups). (*A*) Elevated basal BMP activity and BMP9 responsiveness in chondrocytes. The basal BMP activity in $Tgfbr1^{\Delta/\Delta}$ cells is more than 2-fold higher than in control cells (columns 1 and 5). TGFβ1 treatment (2 ng/mL) increases BMP activity in control cells but does not affect $Tgfbr1^{\Delta/\Delta}$ cells (columns 2 and 6). BMP2 (100 ng/mL) and BMP9 (100 ng/mL) have similar activities in control cells at the tested concentrations (columns 3 and 4). BMP9 induces higher BMP activity than BMP2 in $Tgfbr1^{\Delta/\Delta}$ cells (columns 7 and 8). (*B*) NOGGIN does not block elevated basal BMP activity in $Tgfbr1^{\Delta/\Delta}$ cells. Elevated BMP activity in $Tgfbr1^{\Delta/\Delta}$ cells compared with control cells (columns 1 and 5). BMP2 activity in control and $Tgfbr1^{\Delta/\Delta}$ cells (columns 2 and 6). NOGGIN inhibits BMP2 activity in both control and $Tgfbr1^{\Delta/\Delta}$ cells (columns 3 and 4, and columns 7 and 8). NOGGIN does not block elevated basal BMP activity in $Tgfbr1^{\Delta/\Delta}$ cells (columns 5 and 8). (*C*) BMP9 antibody does not block elevated basal BMP activity in $Tgfbr1^{\Delta/\Delta}$ cells. BMP reporter activity is activated by BMP9 in control ATDC5 cells (columns 1 and 2). α-BMP9 antibody blocks exogenous BMP9 action in control and $Tgfbr1^{\Delta/\Delta}$ cells (columns 3 and 7). $Tgfbr1^{\Delta/\Delta}$ cells exhibit elevated basal BMP activity (columns 1 and 5). $Tgfbr1^{\Delta/\Delta}$ cells respond to BMP9 (columns 5 and 6). α-BMP9 antibody has no effect on elevated basal BMP activity in $Tgfbr1^{\Delta/\Delta}$ cells (columns 5 and 8). (*D*) ACVRL1-Fc does not block elevated basal BMP activity in $Tgfbr1^{\Delta/\Delta}$ cells. BMP reporter activity is activated by BMP9 in control ATDC5 cells (columns 1 and 2). ACVRL1-Fc blocks exogenous BMP9 action in control and $Tgfbr1^{\Delta/\Delta}$ cells (columns 3 and 7). $Tgfbr1^{\Delta/\Delta}$ cells exhibit elevated basal BMP activity (columns 1 and 5). $Tgfbr1^{\Delta/\Delta}$ cells respond to BMP9 (columns 5 and 6). ACVRL1-Fc has no effect on elevated basal BMP activity in $Tgfbr1^{\Delta/\Delta}$ cells (columns 5 and 8). (*E*) ACTRIIB-Fc does not block elevated basal BMP activity in $Tgfbr1^{\Delta/\Delta}$ cells. BMP reporter activity is activated by BMP9 in control ATDC5 cells (columns 1 and 2). ACTRIIB-Fc blocks exogenous BMP9 action in control and $Tgfbr1^{\Delta/\Delta}$ cells (columns 3 and 7). $Tgfbr1^{\Delta/\Delta}$ cells exhibit elevated basal BMP activity (columns 1 and 5). $Tgfbr1^{\Delta/\Delta}$ cells respond to BMP9 (columns 5 and 6). ACVRL1-Fc has no effect on elevated basal BMP activity in $Tgfbr1^{\Delta/\Delta}$ cells (columns 5 and 8). (*F*) ACVRL1 antibody blocks elevated basal BMP activity in $Tgfbr1^{\Delta/\Delta}$ cells. BMP reporter activity is activated by BMP9 in control ATDC5 cells (columns 1 and 2). Anti-ACVRL1 antibody does not block BMP9 action in control cells (columns 2 and 4). $Tgfbr1^{\Delta/\Delta}$ cells exhibit elevated basal BMP activity (columns 1 and 5). Anti-ACVRL1 antibody blocks elevated basal BMP activity in $Tgfbr1^{\Delta/\Delta}$ cells (columns 5 and 7). Anti-ACVRL1 antibody restores BMP9 activity to control level in $Tgfbr1^{\Delta/\Delta}$ cells (columns 2, 4, and 8). (*G*) Loss of ACVRL1 kinase activity restores BMP signaling to normal level in the $Tgfbr1^{\Delta/\Delta}$ cells. Elevated BMP activity in $Tgfbr1^{\Delta/\Delta}$ cells compared with control cells (columns 1 and 3). Mutation of threonine-196 to valine near the canonical start of the ACVRL1 kinase domain ($Acvrl1^{KD}$) using Crispr-Cas9 system in the $Tgfbr1^{\Delta/\Delta}$ cells (column 5); BMP activity in *Tgfbr1/Acvrl1* double-mutant cells is restored to normal (columns 1 and 5). BMP9 activity in control and $Tgfbr1^{\Delta/\Delta}$ cells (columns 2 and 4). BMP9 activity in *Tgfbr1/Acvrl1* double-mutant cells is lower than $Tgfbr1^{\Delta/\Delta}$ cells and restored to control levels (columns 2, 4, and 6). (*H*) Anti-ACTRIIB antibody blocks elevated basal BMP activity in $Tgfbr1^{\Delta/\Delta}$ cells. BMP reporter activity is activated by BMP9 in control ATDC5 cells (columns 1 and 2). Anti-ACTRIIB antibody deceases BMP9 action in control cells (columns 2 and 4). $Tgfbr1^{\Delta/\Delta}$ cells exhibit elevated basal BMP activity (columns 1 and 5). Anti-ACTRIIB antibody blocks elevated basal BMP activity in $Tgfbr1^{\Delta/\Delta}$ cells (columns 5 and 7). Anti-ACTRIIB antibody decreases BMP9 activity by 2-fold in $Tgfbr1^{\Delta/\Delta}$ cells (columns 6 and 8) but does not completely restore BMP9 activity to control levels (columns 4 and 8).

expression of ligands inhibited by NOGGIN (BMPs 2, 4, 5, and 7, or GDFs 5 to 7), or BMPs 9 and 10.

Anti-ACVRL1 antibody was used to test whether the increased basal and BMP9-induced BMP signaling is mediated directly by ACVRL1 in $Tgfbr1^{\Delta/\Delta}$ cells. In control cells, anti-ACVRL1 has no impact (Fig. 6 *F*, columns 3 and 4). However, in $Tgfbr1^{\Delta/\Delta}$ cells, anti-ACVRL1 blocks both elevated basal BMP activity and responsiveness to BMP9 (Fig. 6 *F*, columns 7 and 8). The basis for the lack of effect of anti-ACVRL1 in control cells is unclear but may be a consequence of sequestration of ACVRL1 by TGFβRI (Fig. 5) into inactive signaling complexes. According to this scenario, the observed responsiveness to BMP9 in control cells may be mediated by ACVR1 rather than ACVRL1. Nonetheless, these results show that ACVRL1 is responsible for increased BMP activity in $Tgfbr1^{\Delta/\Delta}$ cells. To confirm this, the kinase domain in ACVRL1 was mutated by replacing threonine-196 with valine using Crispr-Cas9 in $Tgfbr1^{\Delta/\Delta}$ cells. Loss of ACVRL1 kinase activity rescues both basal BMP activity and responsiveness to BMP9 in $Acvrl1K^{KD}/Tgfbr1^{\Delta/\Delta}$ cells (Fig. 6*G*), confirming that activation of ACVRL1 causes increased BMP signaling in $Tgfbr1^{\Delta/\Delta}$ cells.

Finally, we tested the potential involvement of ACTRIIB in the increased basal and BMP9-induced BMP signaling in $Tgfbr1^{\Delta/\Delta}$ cells. In control cells, anti-ACTRIIB has no impact on basal BMP signaling but deceases BMP9-induced activity (Fig. 6 *H*, columns 3 and 4). In $Tgfbr1^{\Delta/\Delta}$ cells, anti-ACTRIIB blocks elevated basal BMP activity (Fig. 6 *H*, columns 1 and 7). In addition, anti-ACTRIIB blocks most (69%) of BMP9-induced BMP activity (Fig. 6 *H*, columns 6 and 8). The remaining responsiveness to BMP9 is higher than the control level (Fig. 6 *H*,

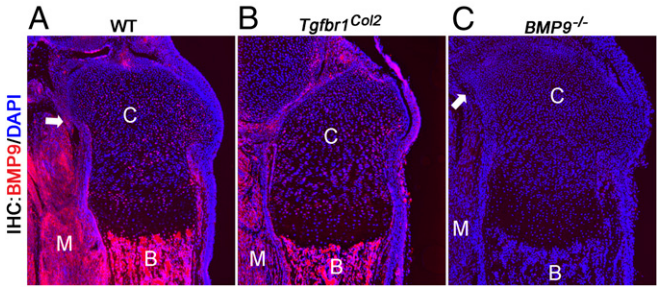

Fig. 7. BMP9 protein is present in growth plate cartilage. Immunofluorescence analysis of WT, $Tgfbr1^{Col2}$, and $Bmp9^{-/-}$ mice to detect the presence of BMP9 in cartilage. WT and $Tgfbr1^{Col2}$ sections are from E18.5 embryos, and $Bmp9^{-/-}$ sections are from P0 newborn pups. α-BMP9 staining is red. Nuclei are stained with DAPI (blue). $n = 3$ mice. (*A* and *B*) In WT and $Tgfbr1^{Col2}$ mice, BMP9 protein is localized in bones as expected. However, BMP9 also presents in the cartilage in these 2 mouse lines. Arrow points to a blood vessel. C, cartilage; B, bone; M, muscle. (*C*) The specificity of anti-BMP9 antibody was validated by using $Bmp9^{-/-}$ mice. No positive signal was detected in $Bmp9^{-/-}$ mice. Arrow points to a blood vessel. C, cartilage; B, bone; M, muscle.

columns 4 and 8). It is unclear whether this is due to only partial blockade of ACTRIIB by the antibody, or to involvement of other type II BMP receptors. Nonetheless, the results indicate that ACTRIIB plays the major role in elevated basal activity and BMP9 responsiveness in $Tgfbr1^{\Delta/\Delta}$ cells, supporting the hypothesis that loss of TGFβRI increases BMP signaling through increased formation of ACVRL1/ACTRIIB complexes.

BMP9 and ACVRL1/ACTRIIB Complexes Are Present in Cartilage of $Tgfbr1^{Col2}$ Mice. The finding that ACVRL1 mediates elevated BMP signaling in *Tgfbr1*-deficient chondrocytes was unexpected because neither ACVRL1 nor its ligands BMP9 and BMP10 have been implicated in growth plate formation. BMP9 and BMP10 are not expressed in normal cartilage (38, 39). In accordance, we did not detect *Bmp9* and *Bmp10* RNA in control or $Tgfbr1^{Col2}$ cartilage by RT-PCR and qPCR (*SI Appendix*, Fig. S2). However, BMP9 and BMP10 circulate in blood (2 to 6 and 0.2 to 2 ng/mL, respectively) in mice (40, 41) at high enough levels to activate ACVRL1. IHC was performed to test whether BMP9 from the circulation or elsewhere can penetrate growth plate cartilage. BMP9 is detected in control and $Tgfbr1^{Col2}$ tissues, with high levels in blood vessels, bone, and muscle, and low levels in cartilage (Fig. 7 *A* and *B*); the specificity of the BMP9 antibody is confirmed by the absence of staining in $Bmp9^{-/-}$ tissue (37) (Fig. 7*C*). These results suggest that BMP9 in cartilage may defuse from nearby vascularized tissues and can potentially activate ACVRL1 in cartilage.

Our in vitro data showed an increase in ACVRL1/ACTRIIB complex formation in $Tgfbr1^{\Delta/\Delta}$ cells, and that these complexes cause elevated BMP activity in $Tgfbr1^{\Delta/\Delta}$ cells. We therefore tested whether we could detect increased ACVRL1/ACTRIIB complex formation in cartilage of $Tgfbr1^{Col2}$ mice using PLA. These complexes are rarely detected in control cartilage but are present in $Tgfbr1^{Col2}$ cartilage (*SI Appendix*, Fig. S3 *A*–*D*).

Discussion

The studies described here demonstrate that TGFβRI is an essential regulator of growth plate chondrocyte proliferation and differentiation. However, TGFβRI, the requisite type I receptor for signal transduction by TGFβs 1 to 3, does not exert its primary function in growth plate chondrocytes via activation of TGFβ pathways. Several lines of evidence support this conclusion. First, the strong $Tgfbr1^{Col2}$ phenotype contrasts with the near absence of growth plate phenotypes in embryos and neonates of $Tgfbr2^{Col2}$ or $Smad2^{Col2}$;$Smad3^{-/-}$ mice (12, 13). Second, the $Tgfbr1^{Col2}$ phenotype is consistent with elevated BMP activity: $Tgfbr1^{Col2}$ mice have a shorter RZ and a longer CZ, associated with an increased proportion of proliferating cells in both regions. This is a hallmark of BMP signaling in chondrocytes (6, 42, 43). Third, pSMAD1/5/8 levels are elevated in $Tgfbr1^{Col2}$ growth plates, and SMADs 1/5/8 play essential roles in activating chondrocyte proliferation in vivo (42). Fourth, pSMAD1/5/8 levels and the majority of the growth plate defects are restored to normal in $Acvrl1/Tgfbr1^{Col2}$ mice.

In addition to the appendicular growth plate phenotype documented here, $Tgfbr1^{Col2}$ mice exhibit axial defects. The axial phenotype appears to be similar to that in $Tgfbr1^{Dermo1}$ mice (19). *Tgfbr1* is highly expressed in intervertebral discs and perichondrium (19). *Col2Cre* is expressed in the sclerotome before the specification of separate lineages for vertebral cartilage and intervertebral discs (44). Since both *Col2Cre* and *Dermo1Cre* would target these tissues, the axial defects in $Tgfbr1^{Col2}$ mice most likely arise through a role for TGFβRI in perichondrium and intervertebral discs. Additional studies employing other genetic models would be needed to define cartilage-intrinsic roles for TGFβRI in vertebral elements. Furthermore, TGFβRI is more widely expressed in posterior condylar tibial cartilage than in anterior condylar tibial cartilage (*SI Appendix*, Fig. S1 *F* and *I*). Consistently, the posterior condyle is smaller than the anterior condyle in $Tgfbr1^{Col2}$ mice. These findings establish *Tgfbr1* as a gene that regulates the differential development of condyles. Evidence for a role for TGFβ signaling in the formation of tendon and ligament insertions has been presented previously. $Tgfbr2^{Prx1}$ mice lack tibial medial condyle and deltoid tuberosity formation (45). However, $Tgfbr2^{Col2}$ mice do not show such phenotypes (12), suggesting that the defects in $Tgfbr2^{Prx1}$ mice are not caused by cells derived from committed chondrocytes. The $Tgfbr1^{Col2}$ defects are distinct from those in $Tgfbr2^{Prx1}$ mice in that $Tgfbr1^{Col2}$ mice have both anterior and posterior condyle defects instead of absence of the medial condyle, and $Tgfbr1^{Col2}$ mice have normal tuberosities. In addition, none of the defects seen in $Tgfbr1^{Col2}$ mice is found in $Tgfbr2^{Col2}$ mice (12). This suggests that *Tgfbr1* regulates posterior and anterior condyle formation in cartilage, but probably not through canonical TGFβ signaling. Scx^{+};$Sox9^{+}$ cells in the TGFβRI-expressing regions of the condyles give rise to ligaments and the ligamentous junction (46). Future studies would thus be of interest to elucidate the role of TGFβRI in the differential development of condyles, ligaments, and associated structures, and to understand the basis for the differing condylar phenotypes in $Tgfbr1^{Col2}$ and $Tgfbr2^{Col2}$ mice.

Our studies unveiled that the excess BMP signaling in $Tgfbr1^{Col2}$ mice is mediated by ACVRL1. A role for TGFβRI as an inhibitor of ACVRL1 function has not been reported previously. Little is known about ACVRL1 function in cartilage, but TGFβRI and ACVRL1 have opposing functions in chondrocytes in vitro (28). The absence of a discernable phenotype in $Acvrl1^{Col2}$ mice indicates that this receptor is dispensable for cartilage development. The loss of TGFβR1 leads to a deleterious gain of function of ACVRL1 signaling in cartilage. This raises the question of the normal function of Acvrl1 in cartilage. Although we have not detected an obvious phenotype in $Acvrl1^{Col2}$ mice at birth, we cannot rule out subtle defects. Examination of adult mice may reveal such changes. Furthermore, it is possible that loss of ACVRL1 is compensated for by the closely related type I BMP receptor ACVR1 (ALK2). Like ACVRL1, ACVR1 is activated by BMPs 9 and 10 (8). $Acvr1^{Col2}$ mice are viable and exhibit only mild appendicular defects (47). Removing both *Acvrl1* and *Acvr1* in cartilage might provide evidence for compensatory roles in cartilage.

ACVRL1 has been studied most extensively in the vasculature. $Acvrl1^{-/-}$ mice die at midgestation due to major defects in angiogenesis, and $Acvrl1^{+/-}$ mice and humans exhibit hereditary hemorrhagic telangiectasia, a condition characterized by vascular malformations (26). TGFβRI and ACVRL1 interact physically in endothelial cells, but the functional output is different from the one shown here in cartilage; in endothelium, ACVRL1 antagonizes TGFβRI signaling, and TGFβRI/ACVRL1/TGFβRII complexes activate BMP signaling (21, 28, 48), whereas in cartilage, TGFβRI antagonizes ACVRL1. It is likely that TGFβRI and ACVRL1

have context-specific mutually antagonistic functions. Other studies show that ACVRL1 can act independently of TGFβRI in endothelial cells (49, 50). Studies in multiple cell types would be of interest to understand the basis for the cell type-specific responses to the TGFβRI:ACVRL1 balance.

The functions of TGFβRI and ACVRL1 in adult articular cartilage are unclear. Although $Acvrl1^{Col2}$ mice exhibit no developmental defects, cartilage-specific loss of ACVRL1 might impact the maintenance of articular cartilage in adults. ACVRL1 is expressed in articular chondrocytes (27, 28), and the ACVRL1/TGFβRI ratio increases in aged and osteoarthritic articular cartilage due to decreased TGFβRI expression (28). It will therefore be important to test whether $Acvrl1^{Col2}$ mice are resistant to age-induced osteoarthritis. If so, this could lead to therapeutic options for treatment of osteoarthritis based on inhibition of ACVRL1 activity. A recent study showed that postnatal deletion of TGFβRI in cartilage leads to a strong osteoarthritis phenotype, suggesting direct effects in articular cartilage (51). However, TGFβRI was deleted in young mice, and therefore both growth plate and articular cartilage were targeted. Nonetheless, clear alterations in gene expression were noted in articular cartilage. Expression of *Prg4*, a gene expressed in superficial zone articular chondrocytes and essential for maintenance of boundary lubrication (52–54), is greatly reduced upon postnatal loss of TGFβRI. It will be of great interest to elucidate the mechanism by which TGFβRI mediates Prg4 expression (51). Prg4 can be induced by TGFβ (51, 55, 56), but this may be independent of the canonical pathway involving TGFβRII based on the observation that postnatal loss of TGFβRII in cartilage is protective against osteoarthritis (57). Taken together with studies implicating ACVRL1 in the progression of osteoarthritis (58–60), it is likely that TGFβRI will exert some functions in articular cartilage through direct activation of TGFβ pathways and others via inhibition of BMP signaling through antagonism of ACVRL1. Experiments to test this are underway.

None of the defects in $Tgfbr1^{Col2}$ mice is seen in *Tgfbr2* mutants (12). In accordance, we found that TGFβRII interacts only minimally with TGFβRI and ACVRL1 in chondrocytes; in normal cartilage, TGFβRI and ACVRL1 interact primarily with ACTRIIB and ACTRIIA, respectively. TGFβRI prevents ACVRL1/ACTRIIB complex formation, as demonstrated by the de novo formation of these complexes in $Tgfbr1^{\Delta/\Delta}$ chondrocytes and $Tgfbr1^{Col2}$ growth plates. Our data indicate that ACVRL1/ACTRIIB complexes are responsible for the elevated BMP signaling in $Tgfbr1^{Col2}$ growth plates (*SI Appendix*, Fig. S4). We speculate that elevated BMP activity in vivo arises at least in part because ACVRL1/ACTRIIB complexes bind BMP9 with higher affinity (300×) than ACVRL1/ACTRIIA complexes (29). Cartilage-specific deletion and overexpression of ACTRIIB in normal and $Tgfbr1^{Col2}$ mice would provide a genetic test of this model.

BMPs 9 and 10 are the only ligands that activate ACVRL1 at physiological levels (30) and are potent inducers of chondrogenesis in vitro (61). $Tgfbr1^{\Delta/\Delta}$ cells show greatly enhanced sensitivity to BMP9. Neither BMP9 nor BMP10 has been implicated previously in skeletal development. BMP9 is produced in the liver and is present in the circulation at high enough levels to activate BMP signaling (36, 58, 62). BMP10 is predominantly expressed in the heart and is in the circulation, but at lower levels than BMP9 (40, 63). Although neither BMP9 nor BMP10 is produced in cartilage (*SI Appendix*, Fig. S2) (38, 39), BMP9 protein is present in growth plate chondrocytes. We speculate that the BMP9 in the growth plate is derived from the circulation, as high levels were detected in blood vessels and tissues close to the growth plate. Although the mechanisms are unknown, even large molecules can diffuse through dense cartilage extracellular matrix (64).

We consistently observed elevated basal BMP signaling in $Tgfbr1^{\Delta/\Delta}$ cells. The elevated basal signaling is due to activity of ACVRL1 because it was blocked by a mutation that inactivated ACVRL1 kinase activity. However, we were unable to find evidence that the basal activity is ligand dependent. Experiments were performed under serum-free conditions; NOGGIN, anti-BMP9 antibody, ACVRL1-Fc, or ACTRIIB-Fc did not block the increased basal signaling. NOGGIN binds to BMPs 2 and 4 to 7 and GDFs 5 to 7 at the concentrations used here, but does not block BMP9 and BMP10 (33, 65, 66). ACVRL1-Fc blocks BMP9 and BMP10. ACTRIIB-Fc blocks multiple ligands including activins, GDF8, and GDF11 (67, 68). We cannot rule out an effect due to increased levels of an untested ligand, nor can we rule out an effect mediated by altered levels of expression of BMP receptors. qRT-PCR experiments revealed that levels of *Bmpr1a* are reduced in $Tgfbr1^{Col2}$ chondrocytes (*SI Appendix*, Fig. S2). Although this would typically be expected to reduce BMP signaling, Antebi et al. (69) showed that altering relative levels of BMPs receptors can greatly alter responsiveness to specific ligand pairs, enabling some pairs to switch from an antagonistic to an additive mode. An analysis of responsiveness of $Tgfbr1^{Col2}$ chondrocytes to multiple pairs to BMP ligands will be needed to assess how loss of TGFβRI impacts signaling by multiple ligands through each BMP receptor complex. It is conceivable that the elevated basal BMP activity in $Tgfbr1^{\Delta/\Delta}$ cells involves a ligand-independent effect of ACVRL1. Forced expression of ACVRL1 increases basal BMP activity (30, 70, 71). Fluid flow can trigger ligand-independent activation of BMP signaling in vascular tissues (72), and/or can greatly increase sensitivity of ACVRL1 to BMP9 (73). As cartilage experiences mechanical strain in vivo, it will be of interest to test how mechanical forces impact BMP signaling through ACVRL1 in cartilage.

In summary, contradictory to the paradigm, the major role of TGFβRI in growth plate chondrocytes is not to transduce TGFβ signaling, but rather to block ACVRL1-mediated BMP signaling. It is possible that TGFβRI exerts its effects by blocking ACVRL1-mediated BMP signaling in tissues other than growth plate cartilage.

Materials and Methods

Mouse Lines and Breeding. All procedures involving animals were approved by the Institutional Animal Care and Use Committee of University of California, Los Angeles. Mice were housed in an Association for Assessment and Accreditation of Laboratory Animal Care-accredited facility in accordance with the *Guide for the Care and Use of Laboratory Animals* (74). This study was compliant with all relevant ethical regulations regarding animal research. E12.5–E18.5 embryos from C57BL6 backgrounds were used. Both sexes were used as sex was not determined in embryos. To genotype *Tgfbr1*-flox mice, 3 primers were used: 5′-ATGAGTTATTAGAAGTTGTTT-3′, 5′-ACCCTCTCACTCTTCCTGAGT-3′, and 5′-GGAACTGGGAAAGGAGATAAC-3′, with 55 °C annealing temperature, yielding 350-bp wild-type (WT) and 150-bp flox-inserted mutant bands (75). To genotype *Acvrl1*-flox mice, 2 primers were used: 5′-CCTGGACAGCGACTGTACTAC-3′ and 5′-GCCCCATTGCTCTCCTCAAAC-3′, with 68 °C annealing temperature, yielding 450-bp WT and 350-bp flox-inserted mutant bands (50). To genotype *Col2a1-Cre* mice, 2 primers were used: 5′-TGCTCTGTCCGTTTGCCG-3′ and 5′-ACTGTGTCCAGACCAGGC-3′, with 58 °C annealing temperature, yielding a 800-bp band (44).

IHC and TUNEL Assay. Limb tissues were dissected and fixed in 4% paraformaldehyde in PBS. They were then decalcified with Immunocal (Decal Chemical Corporation) for 3 d at 4 °C, embedded in paraffin, and cut at a thickness of 7 μm. Paraffin sections were deparaffinized and rehydrated by passage through xylene and 100%, 95%, and 70% ethanol. Samples were treated with 1 mg/mL hyaluronidase for 30 min at 37 °C. Sections were blocked with 5% goat or donkey serum, in TBS for 1 h at room temperature and incubated with 1:200 diluted primary antibody at 4 °C overnight. Slides were washed 3 times in TBST for 10 min each and incubated at room temperature for an hour in secondary antibody (1:500) conjugated with fluorescent dyes (Cell Signaling; goat anti-rabbit red, R37117; goat anti-rabbit green, R37116; goat anti-mouse red, A11032) in 1% goat or donkey serum TBST. Slides were washed 3 times in PBST for 10 min each and stained in DAPI (Sigma; D9453) at 0.1 μg/mL for 10 min. Lastly, the slide was mounted in 10 μL of Fluoro-Gel (Electron Microscopy Sciences; 1798510). Primary antibodies included the following: α-TGFβRI (Abcam; 31013), α-ACVRL1 (Santa Cruz; 19546), α-pSMAD1/5/8 (Cell Signaling; 9511S), α-pSMAD2/3 (Cell Signaling; 3108S), α-PCNA (Abcam; 2586S), α-TAK1(Cell Signaling; 4508S), and α-BMP9 (R&D; AF3209). Apoptotic cells were detected by in situ TUNEL assay using the In Situ Cell Death Detection Kit (Sigma; 11684795910) following the manufacturer's instructions. All experiments were repeated on sections from at least 3 embryos of each genotype. All comparisons were between littermates.

Skeletal Preparation and Histology. Whole-mount skeletal preparations ($n = 5$) were performed as described (33). For histological analyses, paraffin sections were produced from E13.5, E16.5, E18.5, and postnatal day 0 (P0) mice. Safranin-O staining was performed as described (76). Heights of RZ, CZ, and HZ were measured directly from images ($n = 4$) taken from each of 4 mice per genotype, and significance was evaluated using Student's 2-tailed t test.

RNA Isolation and qPCR. Limb joint cartilages isolated from E17.5 mice were frozen in liquid nitrogen and smashed to powder. Cartilage powder was then fixed in TRIzol. Total RNA was isolated by the phenol-chloroform method and converted to cDNA. The cDNA was amplified and quantified using SYBR Green reagent (Sigma) in a Stratagene Mx3005P qPCR System (Thermo Scientific). Primer sequences are shown in *SI Appendix*, Table S1.

Co-IP. Immunoprecipitations (IPs) were performed using Pierce Crosslink Magnetic IP/Co-IP kit (Thermo Scientific; 88805). To obtain the lysate solution, confluent ATDC5 cells in 150-mm dishes were fixed in 1% formaldehyde at room temperature for 10 min followed by quenching with 125 mM glycine at room temperature for 5 min. Fixed cells were washed with cold PBS twice. Cells were collected by scraper and centrifuged at 750 × *g* for 4 min and then resuspended in PBS supplemented with protease inhibitors mixture (Thermo Scientific). Cross-linking was performed on the suspended cells using disuccinimidyl suberate (Thermo Scientific) with a final concentration of 2.5 mM. The reaction was allowed to proceed for 30 min at room temperature before quenching with Tris with a final concentration of 20 mM. After centrifugation at 750 × *g* for 4 min, cell pellet was resuspended in 500 μL of IP Lysis Buffer from the kit supplemented with protease inhibitors. Lysate was sonicated in an ice-water bath for cell disruption. After IP was performed with antibodies listed in *SI Appendix*, Table S1. The pull-down products were analyzed by Western blot.

Western Blot Analysis. Protein samples were heated in Laemmli buffer at 95 °C for 5 min. Thirty to 50 μg of protein was subjected to sodium dodecyl sulfate–polyacrylamide gel electrophoresis and transferred onto nitrocellulose membranes. After blocking, the membranes were probed with appropriate primary antibodies and then incubated with specific horseradish peroxidase-conjugated secondary antibodies (Bio-Rad). Immunodetection was performed using enhanced chemiluminescence consistent with the manufacturer's protocol (Thermo Fisher Scientific). The band intensities were quantified and normalized to the corresponding controls. The antibodies used are listed in *SI Appendix*, Table S1.

DNA Transfection and Reporter Assay. ATDC5 cells were plated in 48-well plates at a density of 2.0×10^4 cells per well in Dulbecco's modified Eagle's medium (DMEM) (Corning) containing 10% fetal bovine serum (FBS) and 1% streptomycin/penicillin. After 1 h, the cells were transfected in quadruplicates with PolyJet reagent. In total, 0.05 μg of *Renilla* plasmids (Addgene) and 0.1 μg of 12× SBE-Luc (77) plasmids with 0.75 μL of PolyJet reagent were added per well. The cells were grown overnight at 37 °C with CO_2. Twenty-four hours posttransfection, medium was replaced with serum-free DMEM containing 200 μg/mL ascorbic acid and 1% streptomycin/penicillin. After 3 h of starvation, cells were treated with various ligands, Fc-proteins, and antibodies: TGFβ1, 5 ng/mL (R&D 240-B); BMP2, 200 ng/mL (R&D; 355-BM); BMP9, 100 ng/mL (Biolegend; 553102); NOGGIN, 400 ng/mL (R&D; 1967-NG); anti-BMP9, 400 ng/mL (R&D; MAB3209); ACVRL1-Fc, 400 ng/mL (R&D; 370-AL); ACTRIIB-Fc, 400 ng/mL (R&D; 3725-RB); anti-ACVRL1, 400 ng/mL (Santa Cruz; 19546); and anti-ACTRIIB, 400 ng/mL (Santa Cruz; 25453). Twenty-four hours posttreatment, growth media was removed. Then, the cells were washed with PBS and lysed in 0.1 mL of Passive Lysis Buffer (PLB). Dual-luciferase reporter assay was performed using the Promega kit (E1910) in a FLUOstar Omega system (BMG Labtech) following the manufacturer's instructions. Data are presented as ratios of Luc/*Renilla* activity.

CRISPR-Cas9 Gene Editing. Oligos that target *Tgfbr1* were synthesized and linked to lentiCRISPRv2 (1-vector system) plasmid as described (78). Oligo sequences for *Tgfbr1* were as follows: 5′-CACCGCCTCTTCATTTGGCACACGG-3′ and 5′-AAACCCGTGTGCCAAATGAAGAGGC-3′. ATDC5 cells were seeded in 6-well plates at a density of 1×10^6 cells per well in DMEM containing 10% FBS and 1% penicillin/streptomycin. After 24 h, the cells were transfected with 1 μg of lentiCRISPRv2 plasmid and 3 μL of Lipofectamine (SignaGen) per well. After 2 d of transfection, *Tgfbr1* mutant cells ($Tgfbr1^{\Delta/\Delta}$) were selected with puromycin at 4 μg/mL. Mutation of *Tgfbr1* was confirmed by PCR. The PCR used were 5′-GCTTCGTCTGCATTGCACTT-3′ and 5′-AGGTGGTGCCCTCT-GAAATG-3′. WT allele has a 126-bp PCR product, and *Tgfbr1* deletion-mutant allele has no PCR product. Loss of TGFβRI protein was confirmed by Western blot using anti-TGFβRI antibody (Abcam; ab31013). For generating the *Acvrl1* kinase mutation, ATDC5 cells were transfected with RNA oligos (CRISPR RNA [crRNA] and transactivating crRNA [tracrRNA]) and single-stranded DNA oligonucleotides (ssODNs). crRNA was designed as 5′-UGGUGCAGAGGACGGUAGCUGUUUUAGAGCUAUGCU-3′ and ordered from Integrated DNA Technologies (IDT); tracrRNA was ordered from IDT; ssODN was designed as 5′-GCAGCGGCTCGGGGCTCCCCTTCTTGGTGCAGAGGGTGG-TAGCTCGGCAGGTTGCGCTGGTAGAGTGTGTGG-3′. RNA oligos (crRNA and tracrRNA) were mixed in equimolar concentrations to a final duplex concentration of 50 μM. The mix was heated at 95 °C for 5 min and allowed to cool to room temperature (15 to 25 °C). For each sample, crRNA:tracrRNA (50 μM working solution) was diluted in their respective buffers to a final volume of 6 μL each. $Tgfbr1^{\Delta/\Delta}$ cells were transfected with 6 μL of crRNA:tracrRNA (50 μM), 3 μL of ssODN (100 μM), 1 μL of pLentiCas9-Blast plasmid (0.1 μg/μL; Genscript), and 4 μL of Lipofectamine (SignaGen) per well (24-well plate). After 2 d of transfection, *Acvrl1* mutant cells were screened by single-cell colony culture and PCR. PCR primers targeting the *Acvrl1* mutant allele were designed as 5′-CTAGGACTTCCTGGACAGCG-3′ and 5′-CAGCCCGTTGAGTGCTTACC-3′. Mutation in *Acvrl1* was confirmed by sequencing.

PLA. PLA was performed directly after IHC following manufacturer's instructions (Sigma-Aldrich; Duolink PLA Technology). After blocking, sections were incubated with goat anti-ACVRL1 (5 μg/mL; Santa Cruz; 15946), rabbit anti-TGFβR1 (5 μg/mL; Abcam; 31013), and rabbit anti-ACTRIIB (5 μg/mL; Santa Cruz; 25453) antibodies overnight at 4 °C, followed by incubation with secondary antibodies conjugated with PLA probe at 37 °C for 1 h as recommended by manufacturers. Then, ligation and amplification were performed (Duolink detection kit; orange, 555 nm). Finally, mounting medium with DAPI was used.

Statistical Analysis. Statistical comparisons were made between 2 groups using Student's t test; P values of <0.05 were considered significant. For multiple comparisons, we performed 2-way ANOVA (2 factor with replication) analysis, followed by post hoc tests that uses t test to compare 2 groups and controls the familywise error rate by Bonferroni correction of P values ($0.05/n$, n = number of groups).

ACKNOWLEDGMENTS. $Bmp9^{-/-}$ embryos were shared by Dr. Sabine Bailly. $Acvrl1^{fx/fx}$ mice were provided by Dr. Paul Oh. 12×SBE-Luc reporter was provided by Dr. Di Chen. This work was supported by NIH R01 Grants AR044528 and AR073793 to K.M.L.

1. H. M. Kronenberg, Developmental regulation of the growth plate. *Nature* **423**, 332–336 (2003).
2. L. Yang, K. Y. Tsang, H. C. Tang, D. Chan, K. S. E. Cheah, Hypertrophic chondrocytes can become osteoblasts and osteocytes in endochondral bone formation. *Proc. Natl. Acad. Sci. U.S.A.* **111**, 12097–12102 (2014).
3. W. Wang, D. Rigueur, K. M. Lyons, TGFβ signaling in cartilage development and maintenance. *Birth Defects Res. C. Embryo Today* **102**, 37–51 (2014).
4. J. Shen, S. Li, D. Chen, TGF-β signaling and the development of osteoarthritis. *Bone Res.* **2**, 14002 (2014).
5. A. Spagnoli *et al.*, TGF-β signaling is essential for joint morphogenesis. *J. Cell Biol.* **177**, 1105–1117 (2007).
6. B. S. Yoon *et al.*, BMPs regulate multiple aspects of growth-plate chondrogenesis through opposing actions on FGF pathways. *Development* **133**, 4667–4678 (2006).
7. P. M. van der Kraan, E. N. Blaney Davidson, W. B. van den Berg, Bone morphogenetic proteins and articular cartilage: To serve and protect or a wolf in sheep clothing's? *Osteoarthritis Cartilage* **18**, 735–741 (2010).
8. D. Yadin, P. Knaus, T. D. Mueller, Structural insights into BMP receptors: Specificity, activation and inhibition. *Cytokine Growth Factor Rev.* **27**, 13–34 (2016).
9. X. Guo, X.-F. Wang, Signaling cross-talk between TGF-beta/BMP and other pathways. *Cell Res.* **19**, 71–88 (2009).
10. M. Wu, G. Chen, Y.-P. Li, TGF-β and BMP signaling in osteoblast, skeletal development, and bone formation, homeostasis and disease. *Bone Res.* **4**, 16009 (2016).
11. M. F. Pittenger *et al.*, Multilineage potential of adult human mesenchymal stem cells. *Science* **284**, 143–147 (1999).
12. M. O. Baffi *et al.*, Conditional deletion of the TGF-beta type II receptor in Col2a expressing cells results in defects in the axial skeleton without alterations in chondrocyte differentiation or embryonic development of long bones. *Dev. Biol.* **276**, 124–142 (2004).
13. W. Wang *et al.*, Smad2 and Smad3 regulate chondrocyte proliferation and differentiation in the growth plate. *PLoS Genet.* **12**, e1006352 (2016).
14. X. Yang *et al.*, TGF-β/Smad3 signals repress chondrocyte hypertrophic differentiation and are required for maintaining articular cartilage. *J. Cell Biol.* **153**, 35–46 (2001).
15. J. Iwata *et al.*, Modulation of noncanonical TGF-β signaling prevents cleft palate in Tgfbr2 mutant mice. *J. Clin. Invest.* **122**, 873–885 (2012).

16. A. Rebbapragada, H. Benchabane, J. L. Wrana, A. J. Celeste, L. Attisano, Myostatin signals through a transforming growth factor beta-like signaling pathway to block adipogenesis. *Mol. Cell. Biol.* **23**, 7230–7242 (2003).
17. S. Li *et al*., GDF10 is a signal for axonal sprouting and functional recovery after stroke. *Nat. Neurosci.* **18**, 1737–1745 (2015).
18. O. Andersson, E. Reissmann, C. F. Ibáñez, Growth differentiation factor 11 signals through the transforming growth factor-beta receptor ALK5 to regionalize the anterior-posterior axis. *EMBO Rep.* **7**, 831–837 (2006).
19. T. Matsunobu *et al*., Critical roles of the TGF-beta type I receptor ALK5 in perichondrial formation and function, cartilage integrity, and osteoblast differentiation during growth plate development. *Dev. Biol.* **332**, 325–338 (2009).
20. E. Pardali, M.-J. Goumans, P. ten Dijke, Signaling by members of the TGF-beta family in vascular morphogenesis and disease. *Trends Cell Biol.* **20**, 556–567 (2010).
21. M. J. Goumans *et al*., Activin receptor-like kinase (ALK)1 is an antagonistic mediator of lateral TGFbeta/ALK5 signaling. *Mol. Cell* **12**, 817–828 (2003).
22. J.-H. Shim *et al*., TAK1 is an essential regulator of BMP signalling in cartilage. *EMBO J.* **28**, 2028–2041 (2009).
23. A. Ray, P. N. P. Singh, M. L. Sohaskey, R. M. Harland, A. Bandyopadhyay, Precise spatial restriction of BMP signaling is essential for articular cartilage differentiation. *Development* **142**, 1169–1179 (2015).
24. K. D. Estrada, K. N. Retting, A. M. Chin, K. M. Lyons, Smad6 is essential to limit BMP signaling during cartilage development. *J. Bone Miner. Res.* **26**, 2498–2510 (2011).
25. E. Minina *et al*., BMP and Ihh/PTHrP signaling interact to coordinate chondrocyte proliferation and differentiation. *Development* **128**, 4523–4534 (2001).
26. L. Ruiz-Llorente *et al*., Endoglin and alk1 as therapeutic targets for hereditary hemorrhagic telangiectasia. *Expert Opin. Ther. Targets* **21**, 933–947 (2017).
27. K. W. Finnson, W. L. Parker, P. ten Dijke, M. Thorikay, A. Philip, ALK1 opposes ALK5/Smad3 signaling and expression of extracellular matrix components in human chondrocytes. *J. Bone Miner. Res.* **23**, 896–906 (2008).
28. E. N. Blaney Davidson *et al*., Increase in ALK1/ALK5 ratio as a cause for elevated MMP-13 expression in osteoarthritis in humans and mice. *J. Immunol.* **182**, 7937–7945 (2009).
29. S. A. Townson *et al*., Specificity and structure of a high affinity activin receptor-like kinase 1 (ALK1) signaling complex. *J. Biol. Chem.* **287**, 27313–27325 (2012).
30. L. David, C. Mallet, S. Mazerbourg, J.-J. Feige, S. Bailly, Identification of BMP9 and BMP10 as functional activators of the orphan activin receptor-like kinase 1 (ALK1) in endothelial cells. *Blood* **109**, 1953–1961 (2007).
31. P. ten Dijke *et al*., Characterization of type I receptors for transforming growth factor-beta and activin. *Science* **264**, 101–104 (1994).
32. M. Macías-Silva, P. A. Hoodless, S. J. Tang, M. Buchwald, J. L. Wrana, Specific activation of Smad1 signaling pathways by the BMP7 type I receptor, ALK2. *J. Biol. Chem.* **273**, 25628–25636 (1998).
33. J. Groppe *et al*., Structural basis of BMP signalling inhibition by the cystine knot protein Noggin. *Nature* **420**, 636–642 (2002).
34. C. Krause, A. Guzman, P. Knaus, Noggin. *Int. J. Biochem. Cell Biol.* **43**, 478–481 (2011).
35. S. Ruiz *et al*., A mouse model of hereditary hemorrhagic telangiectasia generated by transmammary-delivered immunoblocking of BMP9 and BMP10. *Sci. Rep.* **5**, 37366 (2016).
36. L. David *et al*., Bone morphogenetic protein-9 is a circulating vascular quiescence factor. *Circ. Res.* **102**, 914–922 (2008).
37. N. Ricard *et al*., BMP9 and BMP10 are critical for postnatal retinal vascular remodeling. *Blood* **119**, 6162–6171 (2012).
38. Y. Wang *et al*., Microarray analysis of proliferative and hypertrophic growth plate zones identifies differentiation markers and signal pathways. *Bone* **35**, 1273–1293 (2004).
39. P. Garrison, S. Yue, J. Hanson, J. Baron, J. C. Lui, Spatial regulation of bone morphogenetic proteins (BMPs) in postnatal articular and growth plate cartilage. *PLoS One* **12**, e0176752 (2017).
40. H. Chen *et al*., Context-dependent signaling defines roles of BMP9 and BMP10 in embryonic and postnatal development. *Proc. Natl. Acad. Sci. U.S.A.* **110**, 11887–11892 (2013).
41. M. Bidart *et al*., BMP9 is produced by hepatocytes and circulates mainly in an active mature form complexed to its prodomain. *Cell. Mol. Life Sci.* **69**, 313–324 (2012).
42. K. N. Retting, B. Song, B. S. Yoon, K. M. Lyons, BMP canonical Smad signaling through Smad1 and Smad5 is required for endochondral bone formation. *Development* **136**, 1093–1104 (2009).
43. B. S. Yoon *et al*., Bmpr1a and Bmpr1b have overlapping functions and are essential for chondrogenesis in vivo. *Proc. Natl. Acad. Sci. U.S.A.* **102**, 5062–5067 (2005).
44. D. A. Ovchinnikov, J. M. Deng, G. Ogunrinu, R. R. Behringer, Col2a1-directed expression of Cre recombinase in differentiating chondrocytes in transgenic mice. *Genesis* **26**, 145–146 (2000).
45. E. Blitz, A. Sharir, H. Akiyama, E. Zelzer, Tendon-bone attachment unit is formed modularly by a distinct pool of Scx- and Sox9-positive progenitors. *Development* **140**, 2680–2690 (2013).
46. Y. Sugimoto *et al*., $Scx^+/Sox9^+$ progenitors contribute to the establishment of the junction between cartilage and tendon/ligament. *Development* **140**, 2280–2288 (2013).
47. D. Rigueur *et al*., The type I BMP receptor ACVR1/ALK2 is required for chondrogenesis during development. *J. Bone Miner. Res.* **30**, 733–741 (2015).
48. F. Curado *et al*., ALK5 and ALK1 play antagonistic roles in transforming growth factor β-induced podosome formation in aortic endothelial cells. *Mol. Cell. Biol.* **34**, 4389–4403 (2014).
49. E. S. Shao, L. Lin, Y. Yao, K. I. Boström, Expression of vascular endothelial growth factor is coordinately regulated by the activin-like kinase receptors 1 and 5 in endothelial cells. *Blood* **114**, 2197–2206 (2009).
50. S. O. Park *et al*., ALK5- and TGFBR2-independent role of ALK1 in the pathogenesis of hereditary hemorrhagic telangiectasia type 2. *Blood* **111**, 633–642 (2008).
51. Q. Wang *et al*., Cartilage-specific deletion of Alk5 gene results in a progressive osteoarthritis-like phenotype in mice. *Osteoarthritis Cartilage* **25**, 1868–1879 (2017).
52. D. K. Rhee *et al*., The secreted glycoprotein lubricin protects cartilage surfaces and inhibits synovial cell overgrowth. *J. Clin. Invest.* **115**, 622–631 (2005).
53. J. M. Coles *et al*., Loss of cartilage structure, stiffness, and frictional properties in mice lacking PRG4. *Arthritis Rheum.* **62**, 1666–1674 (2010).
54. K. A. Waller *et al*., Role of lubricin and boundary lubrication in the prevention of chondrocyte apoptosis. *Proc. Natl. Acad. Sci. U.S.A.* **110**, 5852–5857 (2013).
55. T. Niikura, A. H. Reddi, Differential regulation of lubricin/superficial zone protein by transforming growth factor beta/bone morphogenetic protein superfamily members in articular chondrocytes and synoviocytes. *Arthritis Rheum.* **56**, 2312–2321 (2007).
56. T. Matsuzaki *et al*., FoxO transcription factors modulate autophagy and proteoglycan 4 in cartilage homeostasis and osteoarthritis. *Sci. Transl. Med.* **10**, eaan0746 (2018).
57. R. Chen *et al*., Attenuation of the progression of articular cartilage degeneration by inhibition of TGF-β1 signaling in a mouse model of osteoarthritis. *Am. J. Pathol.* **185**, 2875–2885 (2015).
58. A. van Caam *et al*., The high affinity ALK1-ligand BMP9 induces a hypertrophy-like state in chondrocytes that is antagonized by TGFβ1. *Osteoarthritis Cartilage* **23**, 985–995 (2015).
59. A. van Caam *et al*., Expression of TGFβ-family signalling components in ageing cartilage: Age-related loss of TGFβ and BMP receptors. *Osteoarthritis Cartilage* **24**, 1235–1245 (2016).
60. A. van Caam *et al*., TGFβ1-induced SMAD2/3 and SMAD1/5 phosphorylation are both ALK5-kinase-dependent in primary chondrocytes and mediated by TAK1 kinase activity. *Arthritis Res. Ther.* **19**, 112 (2017).
61. P. Seemann *et al*., Mutations in GDF5 reveal a key residue mediating BMP inhibition by NOGGIN. *PLoS Genet.* **5**, e1000747 (2009).
62. B. Herrera, G. J. Inman, A rapid and sensitive bioassay for the simultaneous measurement of multiple bone morphogenetic proteins. Identification and quantification of BMP4, BMP6 and BMP9 in bovine and human serum. *BMC Cell Biol.* **10**, 20 (2009).
63. H. Neuhaus, V. Rosen, R. S. Thies, Heart specific expression of mouse BMP-10 a novel member of the TGF-beta superfamily. *Mech. Dev.* **80**, 181–184 (1999).
64. C. D. DiDomenico, L. J. Bonassar, How can 50 years of solute transport data in articular cartilage inform the design of arthritis therapeutics? *Osteoarthritis Cartilage* **26**, 1438–1446 (2018).
65. L. B. Zimmerman, J. M. De Jesús-Escobar, R. M. Harland, The Spemann organizer signal noggin binds and inactivates bone morphogenetic protein 4. *Cell* **86**, 599–606 (1996).
66. H. N. Beck, K. Drahushuk, D. B. Jacoby, D. Higgins, P. J. Lein, Bone morphogenetic protein-5 (BMP-5) promotes dendritic growth in cultured sympathetic neurons. *BMC Neurosci.* **2**, 12 (2001).
67. D. Sako *et al*., Characterization of the ligand binding functionality of the extracellular domain of activin receptor type IIb. *J. Biol. Chem.* **285**, 21037–21048 (2010).
68. F. Morvan *et al*., Blockade of activin type II receptors with a dual anti-ActRIIA/IIB antibody is critical to promote maximal skeletal muscle hypertrophy. *Proc. Natl. Acad. Sci. U.S.A.* **114**, 12448–12453 (2017).
69. Y. E. Antebi *et al*., Combinatorial signal perception in the BMP pathway. *Cell* **170**, 1184–1196.e24 (2017).
70. A. Lux, L. Attisano, D. A. Marchuk, Assignment of transforming growth factor beta1 and beta3 and a third new ligand to the type I receptor ALK-1. *J. Biol. Chem.* **274**, 9984–9992 (1999).
71. F. J. Blanco *et al*., Interaction and functional interplay between endoglin and ALK-1, two components of the endothelial transforming growth factor-beta receptor complex. *J. Cell. Physiol.* **204**, 574–584 (2005).
72. J. Zhou *et al*., Force-specific activation of Smad1/5 regulates vascular endothelial cell cycle progression in response to disturbed flow. *Proc. Natl. Acad. Sci. U.S.A.* **109**, 7770–7775 (2012).
73. N. Baeyens *et al*., Defective fluid shear stress mechanotransduction mediates hereditary hemorrhagic telangiectasia. *J. Cell Biol.* **214**, 807–816 (2016).
74. National Research Council, *Guide for the Care and Use of Laboratory Animals* (National Academies Press, Washington, DC, ed. 8, 2011).
75. J. Larsson *et al*., Abnormal angiogenesis but intact hematopoietic potential in TGF-beta type I receptor-deficient mice. *EMBO J.* **20**, 1663–1673 (2001).
76. L. Rosenberg Chemical basis for the histological use of safranin O in the study of articular cartilage. *J. Bone Joint Surg. Am.* **53**, 69–82 (1971).
77. M. Zhao, M. Qiao, B. O. Oyajobi, G. R. Mundy, D. Chen, E3 ubiquitin ligase Smurf1 mediates core-binding factor α1/Runx2 degradation and plays a specific role in osteoblast differentiation. *J. Biol. Chem.* **278**, 27939–27944 (2003).
78. O. Shalem *et al*., Genome-scale CRISPR-Cas9 knockout screening in human cells. *Science* **343**, 84–87 (2014).